The Core/Shell Composite Nanowires Produced by Self-Scrolling Carbon Nanotubes onto Copper Nanowires

Keyou Yan,[†] Qingzhong Xue,[†,*] Dan Xia,[†] Huijuan Chen,[†] Jie Xie,[†] and Mingdong Dong[‡,*]

[†]College of Physics Science and Technology, China University of Petroleum, Dongying, Shandong 257061, P. R. China, and [‡]Rowland Institute at Harvard, Harvard University, 100 Edwin H. Land Boulevard, Cambridge, Massachusetts 02142

ABSTRACT We demonstrated a novel method to produce core/shell composite nanowires (NWs) by self-scrolling carbon nanotubes (CNTs) onto copper NWs *via* forced-field-based molecular dynamic (MD) simulations. When large diameter CNTs are placed beside the copper NWs, the CNTs approach the NWs, collapse, and self-scroll onto the NWs, resulting in coaxial core/shell composite NWs. It is found that the van der Waals force plays an important role in the formation of the composite NWs. The expected outcome of this novel method is to determine various strategies on how to produce composite NWs. Coaxial core/shell composite NWs represent an important class of nanoscale building blocks with substantial potential for exploring new concepts and functional materials.

KEYWORDS: carbon nanotubes · nanowires · self-scrolling · composite nanowires · molecular dynamic simulation

Nanowires (NWs) have attracted significant attention owing to their potential applications including nanosensors and high density electronic and optoelectronic devices.[1−4] In previous works, various metal NWs (gold, silver, and copper) have been synthesized.[5−7] The properties of the NWs are determined by their size, morphology, and composition. Especially, composite NWs can improve the physical and chemical properties of materials, which would allow great flexibility in designing new experiments and developing novel applications. The surface area to volume ratio plays an important role in chemical reactions involving a solid material. NWs have an exceptionally high surface to volume ratio, which provide NW compositions with a high reactivity. Herein, we propose a novel method to produce copper/carbon core/shell composite NWs through self-scrolling carbon nanotubes (CNTs) onto Cu NWs *via* molecular dynamic (MD) simulation. The simulations show that the van der Waals force between CNTs and Cu NWs is the driving force for this self-assembly process. The prospect of core/shell composite NWs is to determine strategies on how to produce composite NWs.

Several ribbon structures of collapsed CNTs have been discovered by Chopra *et al.*, which were synthesized on the surface of Cu cathode by a carbon-arc discharge method. The collapsed CNT arrangement occurred when a conventional hollow cylindrical nanotube was locally deformed by external mechanical forces to form kinked or twisted conformation.[8] The new structures of collapsed CNTs, which provide new structure and new physical properties, have attracted significant attention in the experimental and theoretical studies.[8−21] Successful production of various cross-sectional shapes of CNT, including oval, peanut, and ribbon shapes, under the hydrostatic pressure has introduced a controllable way to produce desired CNT nanostructures.[13−19] In addition, the electrical transitions of deformed CNTs which are sensitive to pressure have provided the opportunity to build nanoscale pressure sensors for practical applications.[13−19] It has also been demonstrated that van der Waals forces between adjacent CNTs can deform their cylindrical symmetry.[22] The flattening of the deformed CNTs along the contact region also implies that the surface contact can also bring deformation of CNTs. Cha *et al.* reported that CNTs can be significantly deformed by metal islands using annular dark-field electron tomography with a scanning transmission electron microscope at nanoscale resolution,[23] which suggested

*Address correspondence to xueqingzhong@tsinghua.org.cn, dong@rowland.harvard.edu.

Received for review June 2, 2009 and accepted July 24, 2009.

Published online August 6, 2009. 10.1021/nn9005818 CCC: $40.75

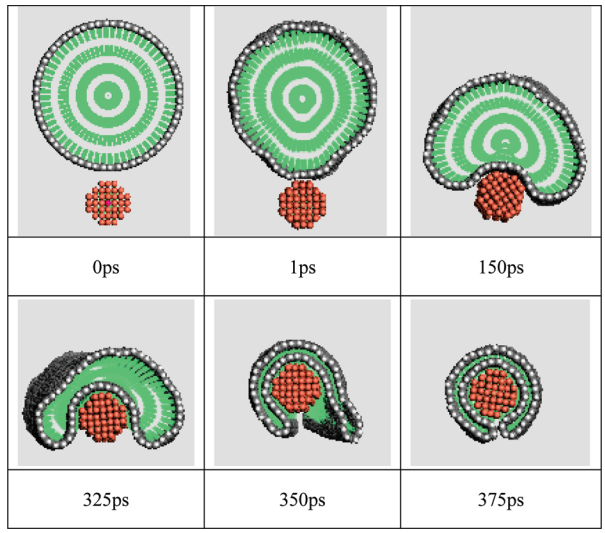

Figure 1. The snapshots of the formation. The CNT (30, 30) collapses to wrap the 12 Å diameter Cu NW core in the simulation.

that the geometric transformation of CNTs can be induced by the metal surface. Clearly, the deformation of CNTs can introduce larger surface contact to some extent. Recently, we found that when the diameters of CNTs reach a certain threshold, the CNTs collapse and form graphene ribbons on the Cu_2O surface.[21] One can expect that the van der Waals force between CNTs and surfaces can be utilized for nanofabrication. The NWs possess even larger specific 3D surface area, which can augment the interaction area comparing to the one in 2D flat surface. A higher deformation can be further introduced by van der Waals force. Here, by introducing Cu NWs to CNTs, we found that the large diameter CNT can easily collapse. Interestingly, the CNTs further scroll around the Cu NW as carbon nanoscrolls (CNS) and eventually form hybrid NWs. The novel core/shell (Cu/CNS) nanostructures can be fabricated by the self-scrolling method, providing a new functionality for NWs.

RESULTS AND DISCUSSION

The formation of Cu/CNS core/shell NWs is simulated by the MD method. The formation in the simulations has two steps. Step 1 is the collapse of CNTs. Step 2 is CNTs scrolling around the Cu NWs. Figure 1 shows some snapshots of the interaction between the CNT (30, 30) with 40.68 Å diameter and 12 Å diameter Cu NW from 0 to 500 ps, respectively. By placing CNTs (30, 30) parallel beside the Cu NW with about 5 Å initial separation, the CNT and the Cu NW approach to each other due to the strong attraction force. During the approaching process, the surface of the CNT which is closer to the Cu NW moves rather faster because carbon atoms closer to Cu NW endure stronger van der Waals force. Therefore, CNT (30, 30) deforms as an oval along the approaching direction as shown in 1 ps snapshot in Figure 1. After the CNT contacts with the Cu NW, the carbon atoms on the topper CNT will keep approaching to the Cu NW due to the attraction force by the van der Waals interaction, which induces the CNTs to collapse to a saddle in the cross-section, as shown in 150 ps snapshot in Figure 1. At 325 ps, when some of the top and bottom atoms of CNT get close enough to each other, the collapse is further accelerated due to the $\pi-\pi$ stack effect between the top layer and bottom layer of the collapsed CNT and then the core/shell (Cu/CNS) nanostructures are produced eventually. (see Supporting Information Videos 1 and 2).

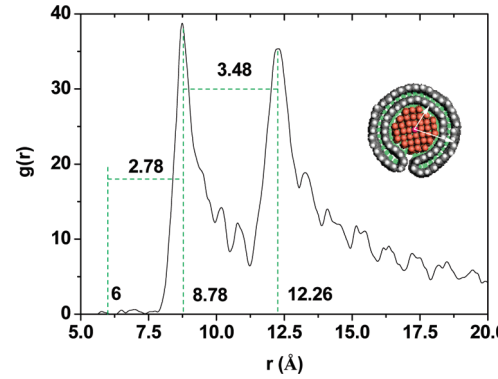

Figure 2. The characteristics of the Cu/CNS structure. The intermolecular pair correlation function between the center Cu atomic wire and the scrolling CNS.

This geometric configuration of the core/shell (Cu/CNS) NW can be further characterized by the intermolecular pair correlation function between the center Cu atomic wire and CNS. From the peak details labeled in Figure 2, the distance between the inner layer of CNS and the center of Cu atomic wire is 8.78 Å, and the distance between the outer layer of CNS and the center of Cu wire is 12.26 Å. As the radii of the Cu NW is 6 Å, the separation between the inner layer of CNS and Cu NW is 2.78 Å, very close to the chemical bond regions, which indicates the interaction between them is very strong.

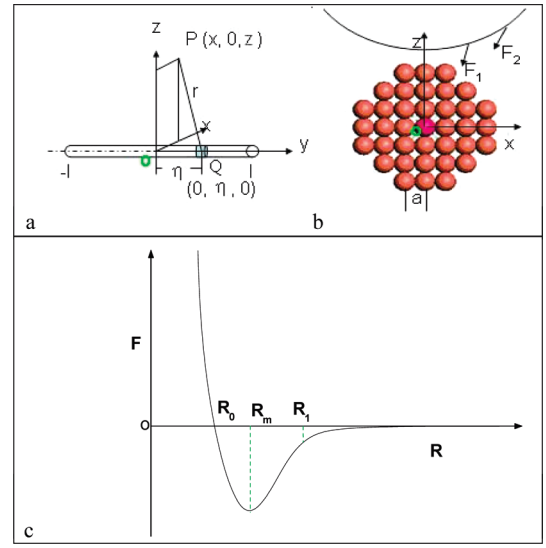

Figure 3. The scheme of the mechanical model: (a,b) the analysis of the interaction of the CNT (30, 30) and 12 Å diameter Cu NW; (c) the force acting on the different points of CNT shell.

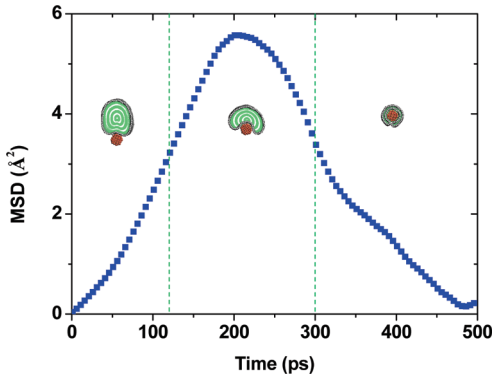

Figure 4. The characteristics of the deformation of the Cu NW; the variation of MSD perpendicular to the approaching direction during the simulation.

The adhesive binding energy between Cu core and CNS shell is -2.05 kcal/mol · Å^2. The distance between the top- and the bottom- CNS layers is 3.48 Å. This is close to the wall thickness of the multiwalled CNTs (3.4 Å). Such CNS can be considered as a double-walled CNT.

Physically, the geometric transformation is determined by the competition between the interaction force experienced and the bending of CNT. Here, we chose a Cu NW consisting of 37 atomic wires along the cross section with the length of 2*l*. We present a mechanical model for the specific CNT−Cu NW system based on Lennard-Jones potential.[24] The CNTs with large diameter can be sufficiently deformed by the interaction force between Cu and carbon atoms. In this specific study system, the analysis of the interaction between the CNT (30, 30) and 12 Å diameter Cu NW is shown in Figure 3a,b. From the Lennard-Jones potential describing the interaction between pairs of atoms, we obtain the differential unit of the potential at $P(x,0,z)$ as shown in eq 1, where ε is the depth of the potential well, σ is the (finite) distance at which the interparticle potential is zero, r is the distance between the particles, a is the distance of two adjacent atom wires, and λ is linear density of the Cu NW. Then we get the potential at $P(x,0,z)$ as shown in eq 2. The force of the atom of CNT

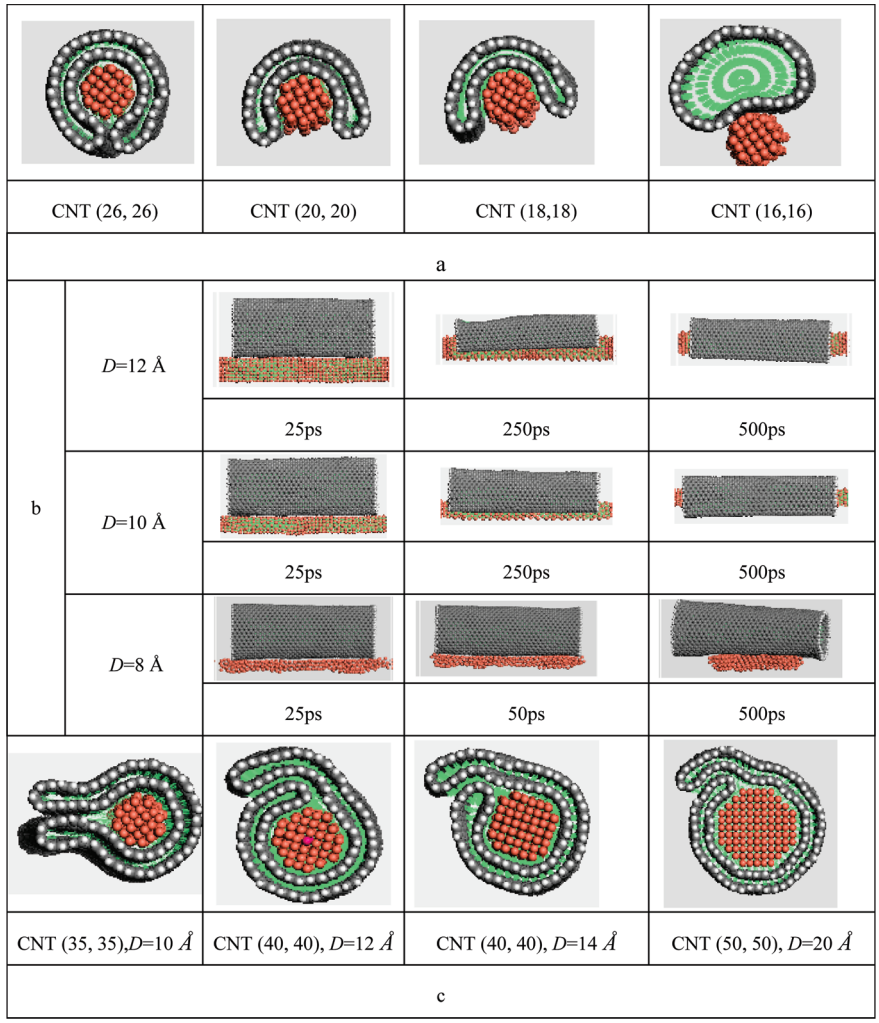

Figure 5. The size effects of the interaction between CNTs and Cu NWs: (a) the interaction between the 10 Å diameter Cu NWs and CNTs with varied diameters; (b) the interaction between the 8 Å diameter Cu NWs with varied diameters and CNT (22, 22); (c) the interaction between Cu NWs and CNTs with larger diameters ($R_{CNT} > D + 8$ Å).

endured from the Cu NW is, of course, the negative gradient of the potential field at $P(x,0,z)$ (eq 3).

$$dU_p = \sum\left(-\frac{A}{r^6}+\frac{B}{r^{12}}\right)\lambda d\eta = -\lambda A\sum_{(i,j=0,0)}^{(3,3),i+j\le 4}\frac{d\eta}{\left[(z\pm ia)^2+(x\pm ja)^2+\eta^2\right]^3}+\lambda B\sum_{(i,j=0,0)}^{(3,3),i+j\le 4}\frac{d\eta}{\left[(z\pm ia)^2+(x\pm ja)^2+\eta^2\right]^6} \quad (1)$$

$$A = 4\varepsilon\sigma^{12},\quad B = 4\varepsilon\sigma^{6}$$

$$U_p = -\lambda A\sum_{(i,j=0,0)}^{(3,3),i+j\le 4}\int_l\frac{d\eta}{\left[(z\pm ia)^2+(x\pm ja)^2+\eta^2\right]^3}+\lambda B\sum_{(i,j=0,0)}^{(3,3),i+j\le 4}\int_l\frac{d\eta}{\left[(z\pm ia)^2+(x\pm ja)^2+\eta^2\right]^6} \quad (2)$$

$$\vec{F} = -\nabla U_p = -\frac{\partial U_p}{\partial x}\vec{i}-\frac{\partial U_p}{\partial z}\vec{k},$$
$$-\frac{\partial U_p}{\partial x} = -6\lambda A\sum_{(i,j)=(0,0)}^{(3,3),i+j\le 4}\int_l\frac{(x\pm ja)d\eta}{\left[(z\pm ia)^2+(x\pm ja)^2+\eta^2\right]^4}+12\lambda B\sum_{(i,j)=(0,0)}^{(3,3),i+j\le 4}\int_l\frac{(x\pm ja)d\eta}{\left[(z\pm ia)^2+(x\pm ja)^2+\eta^2\right]^7} \quad (3)$$
$$-\frac{\partial U_p}{\partial z} = -6\lambda A\sum_{(i,j)=(0,0)}^{(3,3),i+j\le 4}\int_l\frac{(z\pm ia)d\eta}{\left[(z\pm ia)^2+(x\pm ja)^2+\eta^2\right]^4}+12\lambda B\sum_{(i,j)=(0,0)}^{(3,3),i+j\le 4}\int_l\frac{(z\pm ia)d\eta}{\left[(z\pm ia)^2+(x\pm ja)^2+\eta^2\right]^7}$$

As seen from eq 3, the force is mildly attractive as CNT approaches to Cu NW from a distance, but strongly repulsive when they are too close. The distance R between P and the Cu NW can be described as $R = (z^2 + x^2)^{1/2}$. From eq 3, we roughly obtain the trend in the variation of F *vs* R, which is illustrated in Figure 3c with a plot of the force distribution at different points around the Cu NW. The force distribution indicates that when CNT and NW are next to each other, they will approach each other until the interaction reaches minimum ($F = 0$). We assume that M is the bending modulus, a threshold that can just start the deformation of CNTs. When the difference of forces in the adjacent points around the Cu NW is larger than M, the CNTs will deform or even collapse. The mechanical relationship can be described as follows:

$$|dF/dR| > M \quad (4)$$

where $|dF/dR|$ denotes the difference of the endured force per unit distance. When eq 4 is satisfied, the CNT will deform with the interaction force between CNT and Cu NW. It is known that the bending modulus M decreases as CNT diameter increases, which indicates that the larger diameter CNTs are sure to be deformed more easily. In Figure 3c, when the CNT shell is in the regions of $[R_0, R_m]$ and $[R_m, R_1]$, the variations of F along with R are relatively large. The abrupt curve in these two regions indicates the value of $|dF/dR|$ is large enough and the eq 4 will be easily satisfied. That means the radial deformation of the CNT will eventually occur. However, the values of dF/dR are negative and positive in the regions of the $[R_0, R_m]$ and $[R_m, R_1]$, respectively. That indicates the CNTs in the two regions are stretching and shrinking along their cross sections. These results correspond to MD simulation results showing that the different transformations occur in parallel and perpendicular to the approaching direction.

In fact, the deformations happen to not only CNTs, but also Cu NWs because of the strong interaction. The mean squared displacement (MSD) of Cu NW perpendicular to the approaching direction reflects deformation of Cu NW, as shown in Figure 4. Since the Cu NWs are solid cylinders and possess an excellent geometric stability, the NW deformation occurs slightly during the partial scrolling process, which appears as an atomic oscillation in short-range. However, when the collapsed CNTs scroll around the Cu completely, the Cu core restitutes to the normal structures to some extent because of the symmetrical forces along the radial direction.

Figure 5 shows the size effect of the interaction between CNTs and Cu NWs. Figure 5a illustrates the interaction between the 10 Å diameter Cu NWs and the CNTs with varied diameters. We can find that CNT with small diameter, for example CNT (16, 16), cannot collapse fully (see Supporting Information Video 3). Namely, a diameter threshold exists for the collapse of CNT. The collapse and scrolling can happen only if the diameter of CNT is larger than the threshold. Figure 5b shows the interaction between the Cu NWs with varied diameters and CNT (22, 22). In this figure, it can be seen that when the diameter of Cu NW decreases to a small value, for example 8 Å, the Cu NW cannot deform CNT to collapse. Therefore, when the diameter of Cu NW is smaller than the threshold, 8 Å, the Cu NWs cannot keep their own geometric stability, so they cannot deform CNTs to collapse. During size effect study and the geometry configuration analysis, we also obtain the size relationship between CNT and NW roughly as follows:

$$R_{CNT} = D + 8\ \text{Å},\quad (D > 8) \quad (5)$$

where R_{CNT} is the radii of CNT and D is the diameter of NW. $D > 8$ Å indicates that Cu NWs can keep their own geometric stability. If eq 5 is satisfied, the perfect core/shell NW can be produced by scrolling CNT around NW. When $R_{CNT} > D + 8$ Å, there are overlaps of the CNS shell at the suture, as shown in Figure 5c. CNS overlaps back to back when the diameter of the Cu NW core is smaller than 12 Å. However, because larger diameter Cu NWs can provide a larger driving force to scroll the CNSs onto Cu NWs further, CNS overlaps spoon-fashion when the diameter of the Cu NW core is larger than 12 Å.

As well known, CNTs with different chiralities possess different electrical transfer properties ranging from

conductor to semiconductor. In the simulation, the chiralities of CNTs have little effect on the collapse and scrolling. Besides, we also studied the interaction between CNTs and some other metal NWs such as Al, Ag, Fe, Au, and so on and demonstrated that the CNTs can also spontaneously collapse and scroll onto these metal NWs by van der Waals forces. Depending on different chirality of CNTs and different species of metal NWs, the metal NW/CNS architectures produced various heterogeneous core/shell nanostructures, which may bring a wide range of potential applications. For example, because the CNS shells are transparent and metal NWs possess abundant free electrons, when the metal NW/CNSs are served as scaffolds in semiconductor based solar cells, the electron transport will be facilitated and the photocurrent will be enhanced.[25] In addition, the mechanical properties of the metal NW/CNS core/shell composite should be strengthened. On one hand, the metal NWs act as fillers to enhance elasticity of the composite NWs in the radial direction, unlike the soft properties of CNTs in the radial direction.[17] On the other hand, as CNTs are extraordinarily rigid in the axial direction[17] and the radial collapse does not transform the axial structure, CNTs will further enhance the rigidity in the axial direction. Self-scrolling features of CNTs are vastly different from conventional CNTs. The core/shell structures have potential advantages for nanodevice applications such as electronics, sensor, catalysis, thermoelectrics, and optoelectronics. The self-scrolling method is useful as a new approach to fabricating core/shell composite NWs.

METHOD

MD simulations are implemented by the DISCOVER code in MATERIALS STUDIO software. The interatomic interactions are described by the force field of condensed phased optimized molecular potential for atomistic simulation studies (COMPASS).[26] This is *an ab initio* force field that is parametrized and validated using condensed-phase properties in addition to various *ab initio* and empirical data and it has been proven to be applicable in describing the mechanical properties of CNTs.[27,28] The dynamics process is conducted to allow the system to exchange heat with the environment at a constant temperature. The Andersen method[29] is employed in the thermostat to control the thermodynamic temperature and generate the correct statistical ensemble. For a temperature control, the thermodynamic temperature is kept constant by allowing the simulated system to exchange energy with a "heat bath".[29] The force field is expressed as a sum of valence (or bond), cross-terms, and nonbond interactions:

$$E_{total} = E_{valence} + E_{cross-term} + E_{nonbond} \quad (6)$$

$$\begin{aligned} E_{valence} = & \sum_b [K_2(b-b_0)^2 + K_3(b-b_0)^3 + K_4(b-b_0)^4] + \\ & \sum_\theta [H_2(\theta-\theta_0)^2 + H_3(\theta-\theta_0)^3 + H_4(\theta-\theta_0)^4] + \\ & \sum_\phi [V_1[1-\cos(\phi-\phi_1^0)] + V_2[1-\cos(2\phi-\phi_2^0)] + \\ & \qquad V_3[1-\cos(3\phi-\phi_3^0)]] + \\ & \sum_\chi K_\chi \chi^2 + E_{UB} \end{aligned} \quad (7)$$

$$\begin{aligned} E_{cross-term} = & \sum_b \sum_{b'} F_{bb'}(b-b_0)(b'-b_0') + \\ & \sum_\theta \sum_{\theta'} F_{\theta\theta'}(\theta-\theta_0)(\theta'-\theta_0') + \\ & \sum_b \sum_\theta F_{b\theta}(b-b_0)(\theta-\theta_0) + \\ & \sum_b \sum_\phi F_{b\phi}(b-b_0)[V_1\cos\phi + V_2\cos 2\phi + V_3\cos 3\phi] + \\ & \sum_{b'} \sum_\phi F_{b'\phi}(b'-b_0')(b'-b_0')[F_1\cos\phi + F_2\cos 2\phi + F_3\cos 3\phi] + \\ & \sum_\theta \sum_\phi F_{\theta\phi}(\theta-\theta_0)[V_1\cos\phi + V_2\cos 2\phi + V_3\cos 3\phi] + \\ & \sum_\phi \sum_\theta \sum_{\theta'} K_{\phi\theta\theta'}\cos\phi(\theta-\theta_0)\times(\theta'-\theta_0') \end{aligned} \quad (8)$$

$$E_{nonbond} = \sum_{i>j}\left[\frac{A_{ij}}{r_{ij}^9} - \frac{B_{ij}}{r_{ij}^6}\right] + \sum_{i>j}\frac{q_i q_j}{\varepsilon r_{ij}} + E_{H-bond} \quad (9)$$

The valence energy, $E_{valence}$, is generally associated with the terms including bond stretching, valence angle bending, dihedral angle torsion, and inversion. The cross-term interacting energy, $E_{cross-term}$, accounts for the factors such as bond or angle distortions caused by nearby atoms to accurately reproduce the dynamic properties of molecules. The nonbond interaction term, $E_{non-bond}$, which accounts for the interactions between nonbonded atoms, is primarily generated by van der Waals effect. Here, q is the atomic charge, ε is the dielectric constant, and r_{ij} is the $i-j$ atomic separation distance; b and b' are the lengths of two adjacent bonds, θ is the two-bond angle, ϕ is the dihedral torsion angle, and χ is the out of plane angle. b_0, $k_i(i = 2-4)$, θ_0, $H_i(i = 2-4)$, $\phi_i^0(i = 1-3)$, $V_i(i = 1-3)$, $F_{bb'}$, b_0', $F_{\theta\theta'}$, θ_0', $F_{b\theta}$, $F_{b\phi}$, $F_{b'\theta}$, $F_i(i = 1-3)$, $F_{\theta\phi}$, $K_{\phi\theta\theta'}$, A_{ij}, and B_{ij} are fitted from quantum mechanics calculations and implemented into the Discover module of Materials Studio.

MD simulations are performed in periodic boundary conditions in the range of 90.36 × 90.36 × 120.00 Å^3 at 300 K. A time step of 1 fs is used, and data are collected every 1 ps. To study the size effects, we select different diameters of the CNTs and Cu NWs in the simulations. Series of CNTs are aligned parallel to the Cu NWs in the initial models, with separation about 5 Å.

Acknowledgment. This work is supported by 973 National Basic Research Program (2008CB617508), Cultivation Fund of the Key Scientific and Technical Innovation Project, Ministry of Education of China (708061), Program for New Century Excellent Talents in University (NCET-08-0844), and Scientific Research Innovation Foundation of Graduate School of China University of Petroleum.

Supporting Information Available: Video 1: MD simulation showing CNT (30, 30) collapsing and scrolling onto the 12 Å diameter copper nanowire in the cross section. Video 2: MD simulation showing CNT (30, 30) collapsing and scrolling onto the 12 Å diameter copper nanowire in the side view. Video 3: MD simulation showing 10 Å diameter copper nanowire cannot deform CNT (16, 16) to collapse. This material is available free of charge *via* the Internet at http://pubs.acs.org.

REFERENCES AND NOTES

1. Duan, X. F.; Niu, C. M.; Sahi, V.; Chen, J.; Parce, J. W.; Empedocles, S.; Goldman, J. L. High-Performance Thin-Film Transistors Using Semiconductor Nanowires and Nanoribbons. *Nature* **2003**, *425*, 274–278.
2. Lauhon, L. J.; Gudiksen, M. S.; Wang, D. L.; Lieber, C. M. Epitaxial Core−Shell and Core−Multishell Nanowire Heterostructures. *Nature* **2002**, *420*, 57–61.

3. Tian, B.; Zheng, X. L.; Kempa, T. J.; Fang, Y.; Yu, N. F.; Yu, G. H; Huang, J. L.; Lieber, C. M. Coaxial Silicon Nanowires as Solar Cells and Nanoelectronic Power Sources. *Nature* **2007**, *449*, 885–889.
4. Zhou, J. C.; Gao, Y.; Martinez-Molares, A. A.; Jing, X.; Yan, D.; Lau, J.; Hamasaki, T.; Ozkan, C. S.; Ozkan, M.; Hu, E.; Dunn, B. Microtubule-Based Gold Nanowires and Nanowire Arrays. *Small* **2008**, *4*, 1507–1515.
5. Kuo, C. W.; Lai, J. J.; Wei, K. H.; Chen, P. L. Studies of Surface-Modified Gold Nanowires Inside Living Cells. *Adv. Funct. Mater.* **2007**, *17*, 3707–3714.
6. Yen, M. Y.; Chiu, C. W.; Hsia, C. H.; Chen, F. R.; Kai, J. J.; Lee, C. Y.; Chiu, H. T. Synthesis of Cable-like Copper Nanowires. *Adv. Mater.* **2003**, *15*, 235–237.
7. Leach, A. M.; McDowell, M.; Gall, K. Deformation of Top-Down and Bottom-Up Silver Nanowires. *Adv. Funct. Mater.* **2007**, *17*, 43–53.
8. Chopra, N. G.; Benedict, L. X.; Crespi, V. H.; Cohen, M. L.; Louie, S. G.; Zettl, A. Fully Collapsed Carbon Nanotubes. *Nature* **1995**, *377*, 135–138.
9. Xiao, J.; Liu, B.; Huang, Y.; Zuo, J; Hwang, K. C.; Yu, M. F. Collapse and Stability of Single- and Multi-Wall Carbon Nanotubes. *Nanotechnology* **2007**, *18*, 395703−1-7.
10. Chopra, N. G.; Ross, F. M; Zettl, A. Collapsing Carbon Nanotubes With an Electron Beam. *Chem. Phys. Lett.* **1996**, *256*, 241–245.
11. Crespi, V. H.; Chopra, N. G.; Cohen, M. L.; Zettl, A.; Louie, S. G. Anisotropic Electron-Beam Damage and the Collapse of Carbon Nanotubes. *Phys. Rev. B* **1996**, *54*, 5927–5931.
12. Xia, Z.; Riester, L.; Curtin, W. A.; Li, H.; Sheldon, B. W.; Liang, J.; Chang, B.; Xu, J. M. Direct Observation of Toughening Mechanisms in Carbon Nanotube Ceramic Matrix Composites. *Acta. Mater.* **2004**, *52*, 931–944.
13. Zang, J.; Treibergs, A.; Han, Y.; Liu, F. Geometric Constant Defining Shape Transitions of Carbon Nanotubes Under Pressure. *Phys. Rev. Lett.* **2004**, *92*, 105501-1−4.
14. Wu, J.; Zang, J.; Larade, B.; Guo, H.; Gong, X. G.; Liu, F. Computational Design of Carbon Nanotube Electromechanical Pressure Sensors. *Phys Rev. B* **2004**, *69*, 153406-1−4.
15. Tangney, P.; Capaz, R. B.; Spataru, C. D.; Cohen, M. L.; Louie, S. G. Structural Transformations of Carbon Nanotubes Under Hydrostatic Pressure. *Nano Lett.* **2005**, *5*, 2268–2273.
16. Elliott, J. A.; Sandler, J. K. W.; Windle, A. H.; Young, R. J.; Shaffer, M. S. P. Collapse of Single-Wall Carbon Nanotubes is Diameter Dependent. *Phys. Rev. Lett.* **2004**, *92*, 095501-1−4.
17. Sun, D. Y.; Shu, D. J.; Ji, M.; Liu, F.; Wang, M.; Gong, X. G. Pressure-Induced Hard-to-Soft Transition of a Single Carbon Nanotube. *Phys. Rev. B* **2004**, *70*, 165417-1−5.
18. Cai, J. Z.; Lu, L.; Kong, W. J.; Zhu, H. W.; Zhang, C.; Wei, B. Q.; Wu, D. H.; Liu, F. Pressure-Induced Transition in Magnetoresistance of Single-Walled Carbon Nanotubes. *Phys. Rev. Lett.* **2006**, *97*, 026402-1−4.
19. Zanf, J.; Aldas-Palacios, O.; Liu, F. MD Simulation of Structural and Mechanical Transformation of Single-Walled Carbon Nanotubes Under Pressure. *Commun. Comput. Phys.* **2007**, *2*, 451–465.
20. Liu, B.; Yu, M. F.; Huang, Y. G. Role of Lattice Registry in the Full Collapse and Twist Formation of Carbon Nanotubes. *Phys. Rev. B* **2004**, *70*, 161402-1−4.
21. Yan, K. Y.; Xue, Q. Z.; Zheng, Q. B.; Xia, D.; Chen, H. J.; Xie, J. Radial Collapse of Single-Walled Carbon Nanotubes Induced by the Cu_2O Surface. *J. Phys. Chem. C* **2009**, *113*, 3120–3126.
22. Ruoff, R. S.; Tersoff, J.; Lorents, D. C.; Subramoney, S.; Chan, B. Radial Deformation of Carbon Nanotubes by van der Waals Forces. *Nature* **1993**, *364*, 514–516.
23. Cha, J. J.; Weyland, M.; Briere, J. F.; Daykov, I. P.; Arias, T. A.; Muller, D. A. Three-Dimensional Imaging of Carbon Nanotubes Deformed by Metal Islands. *Nano. Lett.* **2007**, *7*, 3770–3774.
24. Lennard-Jones, J. E. Cohesion. *Proc. Phys. Soc.* **1931**, *43*, 461–482.
25. Kongkanand, A.; Domnguez, R. M.; Kamat, P. V. Single Wall Carbon Nanotube Scaffolds for Photoelectrochemical Solar Cells Capture and Transport of Photogenerated Electrons. *Nano Lett.* **2007**, *7*, 676–680.
26. Sun, H. COMPASS: An ab Initio Force-Field Optimized for Condensed-Phase Applications Overview with Details on Alkane and Benzene Compounds. *J. Phys. Chem. B* **1998**, *102*, 7338–7364.
27. Wang, Q.; Duan, W. H.; Liew, K. M.; He, X. Q. Inelastic Buckling of Carbon Nanotubes. *Appl. Phys. Lett.* **2007**, *90*, 033110-1−3.
28. Wang, Q. Atomic Transportation *via* Carbon Nanotubes. *Nano. Lett.* **2009**, *9*, 245–249.
29. Andersen, H. C. MDs Simulations at Constant Pressure and/or Temperature. *J. Chem. Phys.* **1980**, *72*, 2384–2393.